Analytical and Bioanalytical Chemistry (2022) 414:6441–6453
https://doi.org/10.1007/s00216-022-04201-5

RESEARCH PAPER

A highly sensitive strategy for glypican-3 detection based on aptamer/gold carbon dots/magnetic graphene oxide nanosheets as fluorescent biosensor

Guiyin Li[1,2] · Wei Chen[1] · Danhong Mi[1] · Bo Wang[1] · HaiMei Li[1] · Guangxiong Wu[1] · Ping Ding[3] · Jintao Liang[1] · Zhide Zhou[1]

Received: 19 March 2022 / Revised: 30 May 2022 / Accepted: 24 June 2022 / Published online: 5 July 2022

Abstract

Hepatocellular carcinoma (HCC) is the second leading cause of cancer-related deaths in China. Glypican-3 (GPC3) is a specific antigen related to HCC, which is widely used in clinical detection as a reliable marker of HCC. In this paper, a highly sensitive homogeneous apatasensor was designed for GPC3 detection based on fluorescence resonance energy transfer (FRET) where the GPC3 aptamer labelled gold carbon dots (AuCDs-$GPC3_{Apt}$) are used as a donor and magnetic graphene oxide (Fe_3O_4/GO) nanosheets are used as an acceptor. A one-step hydrothermal method was used to synthesize AuCDs to provide sufficient fluorescence. The FRET phenomenon exists between AuCDs-$GPC3_{Apt}$ and Fe_3O_4/GO, which weakens the fluorescence intensity of the whole system. When the target GPC3 is added to the FRET system, the fluorescent AuCDs-$GPC3_{Apt}$ binds to the GPC3 and forms a folded structure, which leads to AuCDs-$GPC3_{Apt}$ separation from Fe_3O_4/GO nanosheets. The Fe_3O_4/GO is then magnetically separated so that the fluorescence of free labelled AuCDs-$GPC3_{Apt}$ is restored. Under the optimum conditions, the fluorescence recovery rate is linearly correlated with the concentration of GPC3 (5–100 ng·mL^{-1}) and the detection limit is 3.01 ng·mL^{-1} (S/N = 3). This strategy shows recoveries from 98.76 to 101.29% in real human serum samples and provides an immediate and effective detection method for the quantification of GPC3 with great potential applications for early diagnosis of HCC.

Keywords Glypican-3 · Fluorescence resonance energy transfer · Magnetic graphene oxide · Gold carbon dots · Fluorescence aptasensor

Introduction

Hepatocellular carcinoma (HCC) is the major histological subtype among types of primary liver cancer and is the second leading cause of cancer-related deaths in China [1]. Due to tumor heterogeneity and distant metastasis, the cure rate of patients with advanced HCC is not optimistic, while clinical studies have demonstrated that the survival rate of patients with early-stage HCC is greatly increased if they are treated promptly [2]. Therefore, strategies to screen for and diagnose early HCC are urgently needed [3]. Serological levels of alpha-fetoprotein (AFP) are commonly used as a classical marker in the field of hepatocellular carcinoma detection [4], but assays targeting AFP have been difficult to meet the requirements of modern medicine for HCC diagnosis in terms of specificity and relevance [5].

Glypican-3 (GPC3) is a transmembrane proteoglycan anchored to the cell membrane by glycosylated

✉ Ping Ding
pingshui@csu.edu.cn

✉ Jintao Liang
dxljt@guet.edu.cn

✉ Zhide Zhou
zzdlgy@163.com

[1] School of Life and Environmental Sciences, Guilin University of Electronic Technology, Guilin, Guangxi 541004, People's Republic of China

[2] College of Chemistry, Guangdong University of Petrochemical Technology, Guandu Road, Maoming, Guangdong 525000, People's Republic of China

[3] Xiang Ya School of Public Health, Central South University, Changsha, Hunan 410078, People's Republic of China

phosphatidylinositol (GPI) [6]. GPC3 has been verified to be closely correlated to the growth, proliferation, invasion, and metastasis of cancer cells [7]. Increasing evidence indicates that its gene is a potential target for promoting HCC cell apoptosis and inhibiting metastasis through the Wnt/beta-catenin and Hh singling pathways [8, 9]. GPC-3 can be actively expressed in hepatoma cells, acting as both tumor promoters and inhibitors in a cancer type-specific manner. Thus, serum GPC3 level can be used as an excellent liver cancer marker to accurately detect HCC. There are various methods to detect GPC3, among which electrochemical measurement [10], luminescence immunoassay [11], and immunological diagnosis [12] are the mainstream ones. However, these methods either have high requirements for equipment or the detection process is cumbersome, which cannot be detected in time and effectively. Herein, we propose an aptamer-based sensor to overcome the above shortcomings and accurately detect the target protein.

Compared with common biomarkers detection methods such as PCR (polymerase chain reaction), immunohistochemistry, and flow cytometry, the biosensor constructed by aptamer (i.e., aptasensors) has the advantages of microscale, rapid response, low detection cost, and micro-detection [13–15]. Aptamers are artificially synthesized single-stranded RNA or DNA oligonucleotide and selected using random libraries in the standard systematic evolution of ligands by exponential enrichment (SELEX) [16]. Aptamer has a high affinity to relevant targets for forming a spatial structure with specific functions, which ensures higher accuracy compared with other biorecognition elements [17]. Related studies show that colorimetric transducers, fluorescent, and electrochemical analysis can greatly improve the detection accuracy after combining with aptamers. As a widely used technology, fluorescence aptasensor has excellent properties such as low cost, simple operation, and high sensitivity [18–20]. In particular, the theory of fluorescence resonance energy transfer (FRET) has been adopted to recognize subtle changes in fluorescence, where energy transfer occurs between fluorescence particles (fluorescence dyes, carbon quantum dots, and UCNPs) as the donors and quenching materials (gold nanoparticles, graphene, and dyes) as the acceptors within a distance less than 10 nm [21, 22]. For instance, Gong et al. constructed a simple and sensitive two-photon imaging fluorescent nitrogen-doped carbon dots (N-CDs) platform which can visually monitor anticancer drug loading by FRET [23]. He et al. developed an intracellular DNA nanoprobe called DNA tetrahedron nanotweezers (DTNT), which can reliably image tumor-related genes in living cells based on the "off" to "on" signal readout mode of FRET [24].

Graphene oxide (GO) is the oxidation product of graphene and is the thinnest material in the universe and has attracted huge attention in recent years [25]. GO has a huge surface area and a large number of functional groups including hydroxyl, epoxy groups, and carboxyl groups, which provide abundant attachment sites for the functionalization [26, 27]. In addition, magnetic Fe_3O_4 nanoparticles have many excellent properties such as low toxicity, biocompatibility, strong magnetism, and catalytic behavior, which makes it a suitable candidate material for biomedical hybrid material [28, 29]. Therefore, it is expected that supported GO on magnetic nanoparticles (i.e., magnetic graphene oxide (Fe_3O_4/GO)) would have profound effects on the performance compared to bared Fe_3O_4 nanoparticles or especially pure GO. On the one hand, GO played a "flexible confinement" function to prevent the agglomeration of pulverized Fe_3O_4. On the other hand, the magnetic Fe_3O_4/GO nanohybrids improved the sensitivity of the detection method contributed to the process of magnetic enriching and separation. Many fluorescence aptasensors with Fe_3O_4/GO nanohybrids as quenchers show excellent detection performance [30–32]. For example, Li et al. presented a fluorometric Hg(II) detection based on the method of magnetic graphene oxide (Fe_3O_4/GO) as a quencher and preconcentrators. The fluorescence of thymine (T) rich ssDNA labelled with naphthalimide derivative is quenched by Fe_3O_4/GO due to FRET [32].

Rhodamine, upconversion nanomaterials (UCNPs), and nucleic acid fluorescent dyes are all commonly used as fluorescence probe for detection. Although rhodamine has high fluorescence intensity, it is inherently toxic and extremely harmful to humans which is not suitable for routine experimental research [33]. UCNPs are optically stable but have low quantum yields and poor biocompatibility which can affect the experimental results [34]. Nucleic acid fluorescent dyes require staining of cells and are complicated to operate [35]. Here, it is necessary to find a suitable fluorescence source to support the experiment. Carbon dots (CDs) are a kind of coordinated optical fluorescence nanomaterials because of their excellent emission spectrum controllability, biocompatibility, and easy functionalization [36]. Gold nanoparticles (AuNPs), as another kind of nanomaterial that has the advantages of high biocompatibility and low toxicity, high extinction coefficients, and fluorescence quenching effect, are widely used in the field of fluorescence detection [37]. Gold carbon dots (AuCDs) nanohybrids have the advantages of both AuNPs and CDs, such as high stability, high fluorescence intensity, and large Stokes shift. CDs is used as the main body to ensure a sufficient fluorescence source for the synthesized AuCDs. AuNPs are absorbed onto the surface of CDs can enhance good attachment of AuCDs to aptamers due to high affinity of gold for aptamers [38]. In addition, the AuCDs have a longer fluorescence decay after the AuNPs is attached to the surface of CDs. For instance, Takashi et al. reported the synthesis of N-CDs and found that N-CDs can be used as reducing and stabilizing agents

to reduce chloroauric acid to AuNPs. And the average fluorescence decay of the N-CD–AuNPs nanocomposite (ca. 2.3 ns) was larger than that of the N-CDs (ca. 1.5 ns) [39].

Herein, a FRET-based aptasensor for GPC3 detection was constructed by using gold-carbon dot nanohybrids (AuCDs) labelled GPC3 aptamer as donors and magnetic graphene oxide (Fe_3O_4/GO) as acceptors. The fluorescence-labelled AuCDs-GPC3$_{Apt}$ complex is formed by the combination of mercapto GPC3$_{Apt}$ and AuCDs through Au–S bond and the coordination of the N atoms in the DNA component and the gold ions of the AuCDs. Fe_3O_4/GO not only has the advantages of magnetic Fe_3O_4 nanomaterials but also has excellent detection performance as a strong quencher. The fluorescence-labelled AuCDs-GPC3$_{Apt}$ complex can be adsorbed on the surface of Fe_3O_4/GO nanosheets through the π-π interaction between the surface of the material and the ssDNA base, thus showing an excellent fluorescence quenching effect. With the addition of target protein GPC3, the fluorescent labelled aptamer binds to the GPC3 and forms a folded structure, which leads to separation from Fe_3O_4/GO nanosheets, thus, the fluorescent signal is retained. The concentration of target GPC3 is quantitatively determined by the changes in fluorescence intensity recorded by spectrophotometer before and after the forming of GPC3-GPC3$_{Apt}$ complex.

Experimental

Reagents and materials

GO was purchased from Nano Pioneer Company (Nanjing, China). Hydrated ferrous sulfate ($FeSO_4 \cdot 7H_2O$), polyethylene glycol (PEG-20000), sodium hydroxide, and other substances were supplied by Xilong Chemical Co., Ltd. (Guangzhou, China). Glucose, chloroauric acid ($HAuCI_4$), and sodium citrate tribasic (SCT) were provided by Aladdin Reagents Ltd. (Shanghai, China).

GPC3 protein and thiolated GPC3 aptamer (GPC3$_{Apt}$) (sequence: 5'-SH-C_6-AAAAAAAATACTCAGGGCACT TGCAAGCAATTGTGGTCCCAATGGGCTGAGTAT-3') [40] were obtained from Shanghai Sangon Biotech Co., Ltd. (Shanghai, China). All solutions were prepared with ultrapure water obtained by standard purification treatment (Milli-Pore, Bedford, MA, USA).

Apparatus

Scanning electron microscopy (SEM) images were collected from Quanta 200 field environmental scanning electron microscope (FEICOMPANY, USA). The structure of AuCDs was observed by transmission electron microscopy (TEM, JEM-2100F, Japan). The zeta potential was measured by Malvern Nano ZS90 Zetasizer (Almelo, Netherlands). All ultraviolet absorption spectra were generated within a limited wavelength range of 200–800 nm (UV–vis, UH5300, HITACHI, Japan). Fluorescence measurements were performed on an F-4600 fluorometer (Hitachi Co., Ltd., Japan).

Preparation of the AuCDs and AuCDs-GPC3$_{Apt}$

The AuCDs are synthesized by a one-step hydrothermal method through synthesis of CDs with simultaneous reduction of the gold ions in chloroauric acid ($HAuCl_4$) to gold monomers. Briefly, 30 mg glucose was added into 50 mL distilled water to obtain 0.6 mg·mL^{-1} glucose solution, then 0.01 mol·L^{-1} chloroauric acid ($HAuCl_4$) solution was added to the glucose solution and stirred for 30 min. Next, 0.01 mol·L^{-1} SCT was dropped into the mixed solution and continue stirring for another 5 min to make the mixture more complete. Finally, the mixture was poured into a hydrothermal reactor lined with Teflon and heated at 200 °C for 6 h in a blast drying oven. Upon completion of the reaction, the container was cooled to room temperature and centrifuged at 13,000 r·min^{-1} for 20 min to obtain AuCDs. The AuNPs and CDs have been prepared without added SCT or without added $HAuCl_4$ with the same preparation process.

40 µL 80 nmol·L^{-1} thiolated GPC3 aptamer (GPC3$_{Apt}$) was added to 5.0 mL AuCDs solution and gently stirred in the dark for 4 h at room temperature. The fluorescence-labelled AuCDs-GPC3$_{Apt}$ complex is formed by the combination of thiolated GPC3$_{Apt}$ and AuCDs through Au–S bond, and the van der Waals forces, and the coordination of the N atoms in the DNA component and the gold ions of the AuCDs. Then separating the coupled AuCDs-GPC3$_{Apt}$ from the uncoupled by centrifuging at 10,000 rpm for about 30 min. Finally, redispersing the residue in 1.0 mL ultrapure water.

Preparation of Fe_3O_4/GO nanosheets>

30 mg GO was dispersed in 7.5 mL deionized water dissolved with 0.6255 g $FeSO_4 \cdot 7H_2O$ by ultrasonic dispersion. 2.5 mL PEG-20000 solution (50 g·L^{-1}) was dissolved into the mixed solution and stirred vigorously at 30 °C. After uniform mixing, dilute ammonia water (0.625 mL concentrated ammonia water, 7.5 mL deionized water) was slowly added to pH = 10 so that Fe^{2+} was precipitated in the form of $Fe(OH)_2$, which was dark green. Then, 67.5 µL H_2O_2 solution was added slowly while stirring for 20 min. After that, the mixed solution was transferred into a high-pressure reaction kettle with a reaction of 160 °C for 5 h. After natural cooling, the product after magnetic separation was thoroughly washed with deionized water and absolute ethyl alcohol in sequence. The product was dried overnight in a

vacuum drying oven at 70 °C. Finally, grinding the product in a mortar to obtain Fe_3O_4/GO powder.

Construction of the FRET-based aptasensor and detection of GPC3

To construct the FRET-based aptasensor, 400 μL Fe_3O_4/GO (2.0 mg·mL^{-1}) and 400 μL AuCDs-GPC3$_{Apt}$ (80 mmol·L^{-1}) were added to 1600 μL HEPES buffer (20 mmol·L^{-1}, pH = 7.0, containing 5.0 mmol·L^{-1} KCl and 5.0 mmol·L^{-1} $MgCl_2$) and the resulting solution was incubated at 25 °C for 50 min after the shake and mixing. From it, the system solution of AuCDs-GPC3$_{Apt}$-Fe_3O_4/GO FRET was constructed. The fluorescence intensity was recorded as F_0 under scanning with a fluorescence spectrophotometer ($\lambda_{ex/em}$ = 350/440 nm). Uniformly dividing the system solution after measuring the fluorescence intensity was evenly divided into 10 groups. Then, the GPC3 (2 μg·mL^{-1}) was gradually diluted into ten groups (5, 10, 20, 40, 60, 80, 100, 200, 400, and 600 ng·mL^{-1}) with PBS buffer solution (20 mmol·L^{-1}, pH = 7.0, containing 5.0 mmol·L^{-1} KCl and 5.0 mmol·L^{-1} $MgCl_2$). Next, 40 μL GPC3 protein solution (in different concentration) was added to 240 μL AuCDs-GPC3$_{Apt}$-Fe_3O_4/GO FRET system and reacted at 25 °C for 120 min with shaking evenly and the fluorescence intensity was recorded as F_1 under scanning with a fluorescence spectrophotometer ($\lambda_{ex/em}$ = 350/440 nm). The calibration plot between fluorescence recovery rate ($F_1 - F_0$) / F_0 and GPC3 concentration was obtained.

Detection GPC3 in human serum samples

In order to demonstrate the practicality of the proposed method, GPC3 in human serum samples were assayed by the AuCDs-GPC3$_{Apt}$-Fe_3O_4/GO FRET system. We got human serum samples from Guangxi Key Laboratory of Metabolic Disease Research, 924 Hospital of Chinese People's Liberation Army (Guilin, China). 0.5 mL healthy human serum was diluted with HEPES buffer to 5.0 mL volume. Then mixing 2.0 μL of diluted human serum with 2.0 μL GPC3 standard solutions of various concentrations (10.0, 30.0, and 60.0 ng·mL^{-1}) which used as different spiked samples. The different spiked samples were added into AuCDs-GPC3$_{Apt}$-Fe_3O_4/GO FRET system, and detected by fluorescence spectroscopy as described above. Then the fluorescence recovery rate is calculated and the specific content of GPC3 was obtained according to the above calibration plot.

Results and discussion

Characterization of AuCDs

CDs, AuNPs, and AuCDs were synthesized using the same hydrothermal method. The synthesis of AuCDs is to reduce the gold ions in chloroauric acid to gold monomers which is adsorbed on the surface of CDs. Details of their respective properties were investigated using the UV spectra and fluorescence spectra. Figure 1a is the UV spectra of CDs

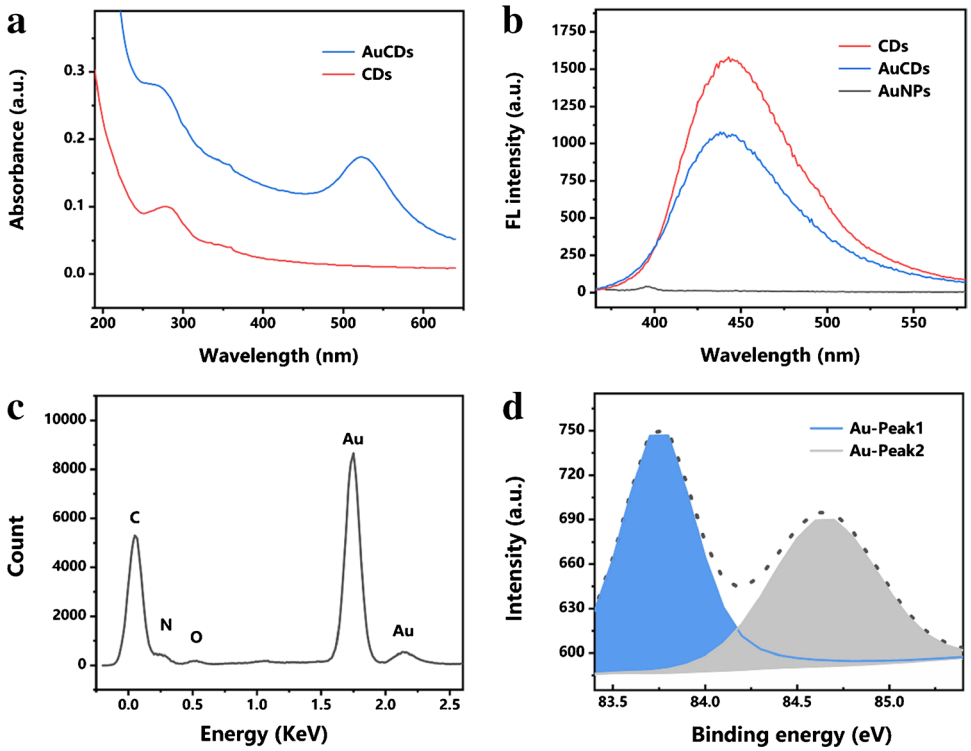

Fig. 1 **a** UV characterization of AuCDs and CDs. **b** Fluorescence emission spectra of AuCDs, CDs, and AuNPs. **c** EDS spectrum of AuCDs. **d** X-ray photoelectron spectroscopy of AuCDs

and AuCDs, and in comparison with CDs, AuCDs have an additional gold absorption peak at 520 nm, which further supports the synthesis of AuCDs. Seen from Fig. 1b, AuNPs have no fluorescence, CDs have strong fluorescence, while AuCDs have less fluorescence. The decrease in fluorescence of the AuCDs confirm that AuNPs have some fluorescence quenching ability [41]. Figure 1c demonstrates the presence of Au element in AuCDs through energy dispersive spectrometer. As shown in XPS spectrum (Fig. 1d), the peak of Au-Peak1 is close to 83.8 eV, while the peak of Au-Peak2 is near to 84.55 eV [42], which further supports that the gold ion is reduce to AuNPs and adsorbed on CDs.

The properties of AuCDs as a fluorescence donor are shown in Fig. 2. The TEM image of AuCDs shows particles are spherical and uniformly dispersed on the contact surface without aggregation, and diameter in the range of 3–7 nm which proves good dispersion (Fig. 2a). The dynamic light scattering measurements revealed that the average size of the AuCDs is near 8 ± 2 nm (Fig. S1a), which is consistent with the size measured by TEM. Under the excitation light source, the electrons in AuCDs generate the motion path of the ground state-excited state-first excited singlet state-ground state, which leads to energy migration and fluorescence emission. The initial excitation spectrum and fluorescence emission spectrum of AuCDs are shown in Fig. 2b, the synthesized AuCDs were excited at 350 nm wavelength, and the fluorescence emission intensity was observed at 440 nm. Compared with the excitation wavelength (EX), the fluorescence emission wavelength (EM) has a redshift, and the Stokes shift of AuCDs is 90 nm. In addition, the fluorescence color of AuCDs is blue under a UV lamp illumination, and the AuCDs solution appears golden yellow under bright light (inset of Fig. 2b).

Characterization of AuCDs-GPC3$_{Apt}$ fluorescence probe

In order to confirm the binding between AuCDs and aptamer, AuCDs-GPC3$_{Apt}$ fluorescence spectrum and ultraviolet absorption spectrum were measured. The fluorescence spectra of AuCDs and AuCDs-GPC3$_{Apt}$ complex are shown in Fig. 2c. Both of AuCDs and AuCDs-GPC3$_{Apt}$ complex have similar fluorescence emission spectra. However, compared to AuCDs, AuCDs-GPC3$_{Apt}$ complex has less fluorescence intensity, and exhibited fluorescence quenching caused by photo-induced electron transfer between AuCDs and aptamer, which may be the cause of the aggregation-disaggregation behavior [43]. AuCDs is disaggregation state and AuCDs-GPC3$_{Apt}$ complex is aggregation state, which could cause the efficient exciton energy transfer from smaller AuCDs to larger aggregates in the complex, leading to the fluorescence quenching in AuCDs-GPC3$_{Apt}$ complex. Nair et al. [44] presented aptamer can quench the fluorescent of sulfur-doped graphene quantum dot (S-GQD) through aggregation-induced quenching of S-GQD with aptamer via S-GQD-aptamer complex formation. On the other hand, it is well known that fluorescence emission occurs when a fluorescence

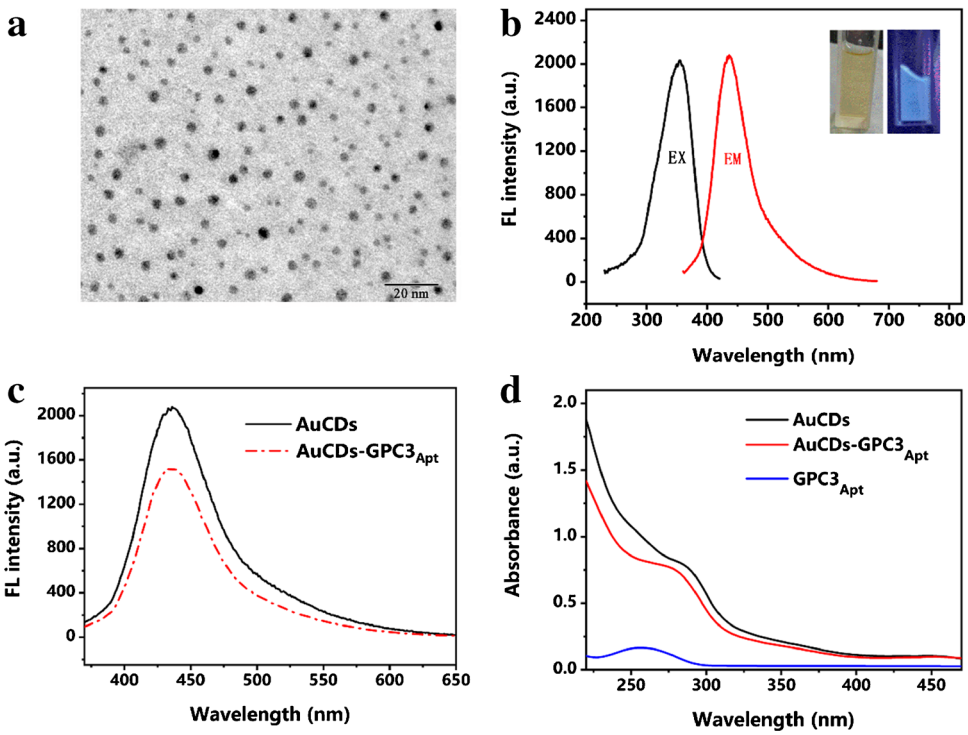

Fig. 2 **a** TEM images of AuCDs. **b** Fluorescence excitation spectrum and emission spectrum of AuCDs (inset is the photograph of AuCDs under a UV lamp illumination and bright light). **c** Fluorescence emission spectra of AuCDs and AuCDs-GPC3$_{Apt}$. **d** Ultraviolet-Vis absorption spectra of AuCDs, AuCDs-GPC3$_{Apt}$, and GPC3$_{Apt}$

substance is irradiated by a specific excitation wavelength. Therefore, the intensity of fluorescence emission is influenced by the intensity of excitation light. When the Au–S bond between AuCDs and sulfhydryl-modified $GPC3_{Apt}$ covers the surface of quantum dots, it can weaken the irradiation of external light waves to quantum dots. And the excitation intensity is weakened, the emission intensity is reduced accordingly [45].

The AuCDs and AuCDs-$GPC3_{Apt}$ complex were also characterized using UV–visible spectroscopy. Figure 2d shows that $GPC3_{Apt}$ has a peak at 260 nm and the AuCDs have peaks at 290 nm. When the $GPC3_{Apt}$ aptamer was added, a new peak located at 275 nm appears, indicating the complexation of aptamer with AuCDs which evidences the conjugation of DNA chains.

To ensure that the AuCDs-$GPC3_{Apt}$ complex could be used as fluorescence probe, the stability of the probe was tested in different conditions. It was demonstrated that the probe maintained fluorescence intensity within the same level at different NaCl solution (Fig. S2a, 0.05–1.00 mol·L^{-1}), different pH (Fig. S2b, 6.0–8.0), and different storage time (Fig. S2c, 24–96 h), and the fluorescence intensity of AuCDs-$GPC3_{Apt}$ was basically constant under different conditions, which shows that AuCDs-$GPC3_{Apt}$ has a strong stability and provides broad possibility and reliability for further practical applications.

Characterization of Fe_3O_4/GO nanosheets

In the fluorescence recovery system, substances with strong fluorescence quenching ability can amplify the fluorescence intensity of the "turn on–off" phenomenon in the system, which is conducive to improving the detection performance of the probe. As a fluorescence quenching with superior performance, magnetic Fe_3O_4/GO is produced by immobilizing Fe_3O_4 nanoparticles (NPs) on the surface of GO, which has the advantage of large accessible surface area of GO and the ability to perform magnetic separation [31]. The particle size of Fe_3O_4/GO is around 800 ± 300 nm (Fig. S1b). The typical SEM images of GO and Fe_3O_4/GO are shown in Fig. 3a and Fig. 3b. The GO surface presents a thin film structure (Fig. 3a), and the surface structure of Fe_3O_4/GO shows a characterization picture of a thin film containing particles (Fig. 3b). This shows that the hybrid materials of the two substances have been successfully prepared. Fe_3O_4/GO has a unique adsorption capacity for nucleotides and is easy to form complexes. Therefore, Fe_3O_4/GO has good fluorescence quenching ability and magnetic separation ability.

The Fourier transform infrared (FT-IR) spectra of GO and Fe_3O_4/GO were drawn to detect their functional groups and chemical bonds (Fig. 3c). GO (Fig. 3c, curve black) has a characteristic peak at 1125 cm^{-1} (C–C stretching vibration), 1390 cm^{-1} (CH stretching vibration), and 1650 cm^{-1} (C=C

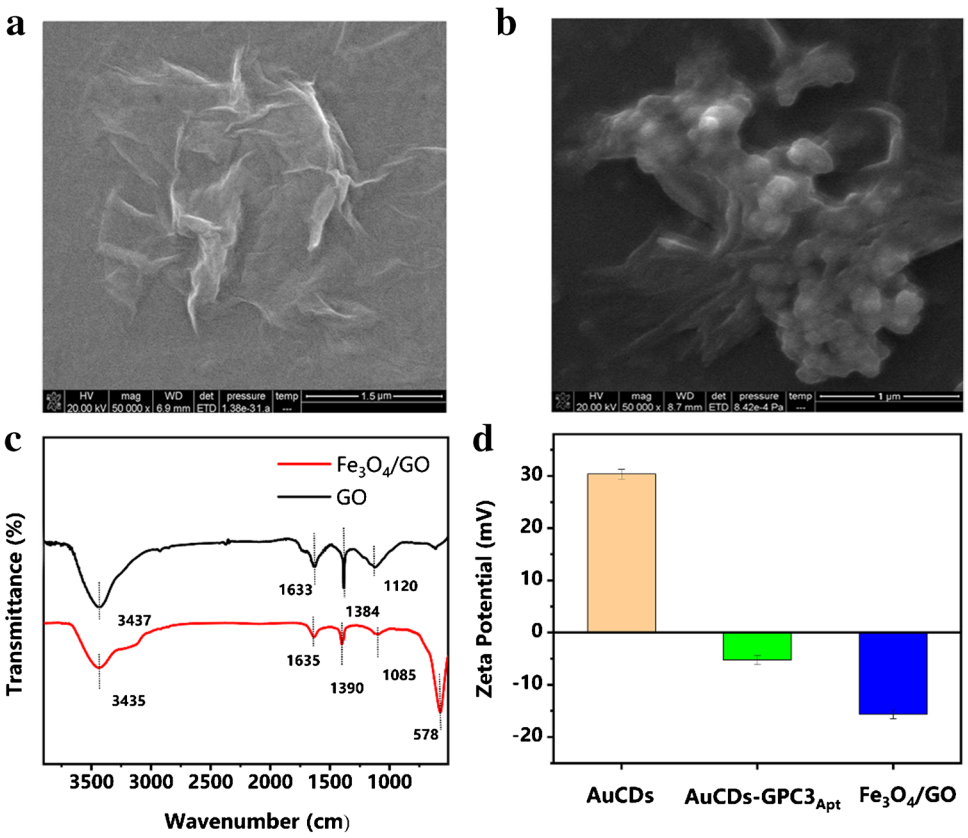

Fig. 3 **a** SEM images of GO. **b** SEM images of Fe_3O_4/GO. **c** Infrared spectrum of GO and Fe_3O_4/GO. **d** Zeta potential of AuCDs, AuCDs-$GPC3_{Apt}$, and Fe_3O_4/GO

stretching) [46]. As a reference, the Fe_3O_4/GO (Fig. 3c curve red) has a new reinforced peak at 578 cm^{-1} which is ascribed to the Fe–O bond stretching vibrations [46]. The zeta potential affects the adsorption amount of charge around particles. As shown in Fig. 3d, the zeta potential of AuCDs, AuCDs-GPC3$_{Apt}$, and Fe_3O_4/GO is 30.37 mV, − 5.23 mV, and − 14.6 mV, which indicates the surface potential of biomass belongs to negative polarity.

Principle of fluorescence aptasensor for GPC3 detection based on Fe_3O_4/GO and AuCDs

The detection strategy of the GPC3 fluorescence aptasensor is shown in Fig. 4a. AuCDs-GPC3$_{Apt}$ was employed as energy donor with Fe_3O_4/GO as energy acceptor to identify GPC3 via FRET process. In this study, the fluorescence AuCDs is manufactured through the hydrothermal method, and sulfhydryl-modified GPC3$_{Apt}$ is combined with AuCDs through gold-sulfur bonds and π-π interactions to form the fluorescently labelled AuCDs-GPC3$_{Apt}$ probe. AuCDs-GPC3$_{Apt}$ probe can be adsorbed on the surface of Fe_3O_4/GO via π-π stacking interactions between Fe_3O_4/GO nanosheets and nucleotide base [47], and the phenomenon of FRET occurs, resulting in the fluorescence of AuCDs-GPC3$_{Apt}$ quenching. When the target protein GPC3 is added to the above AuCDs-GPC3$_{Apt}$-Fe_3O_4/GO system, GPC3 selectively binds to the aptamer of AuCDs-GPC3$_{Apt}$ complex to form Apt-GPC3, leading to the AuCDs-GPC3$_{Apt}$ detached from the Fe_3O_4/GO nanosheets, thereby resulting in significant

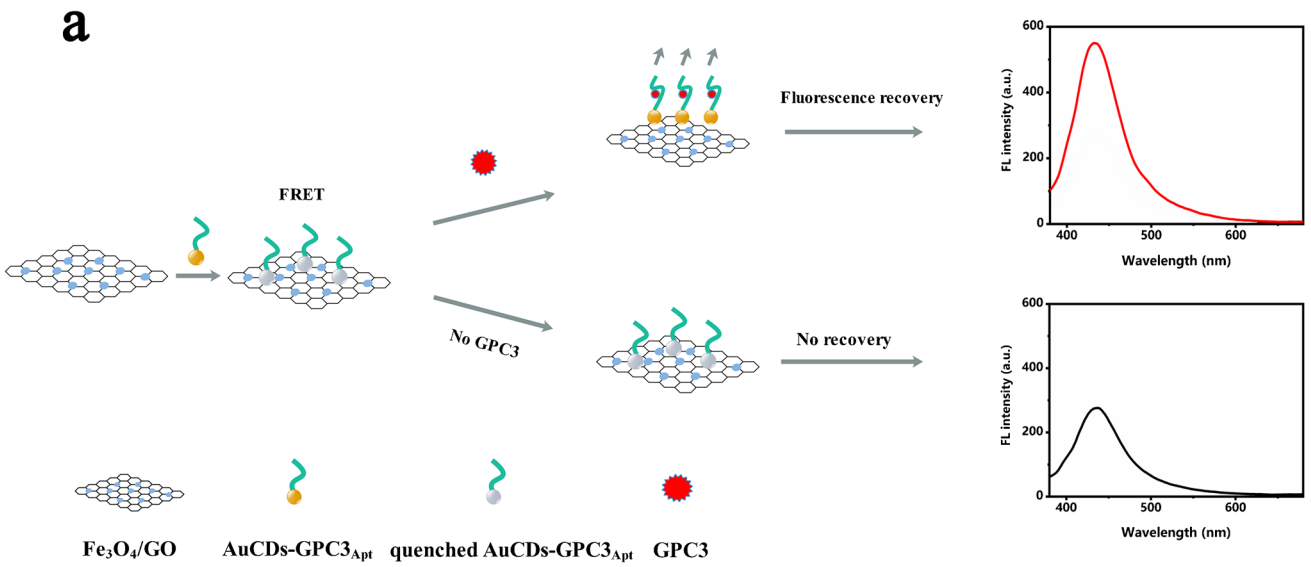

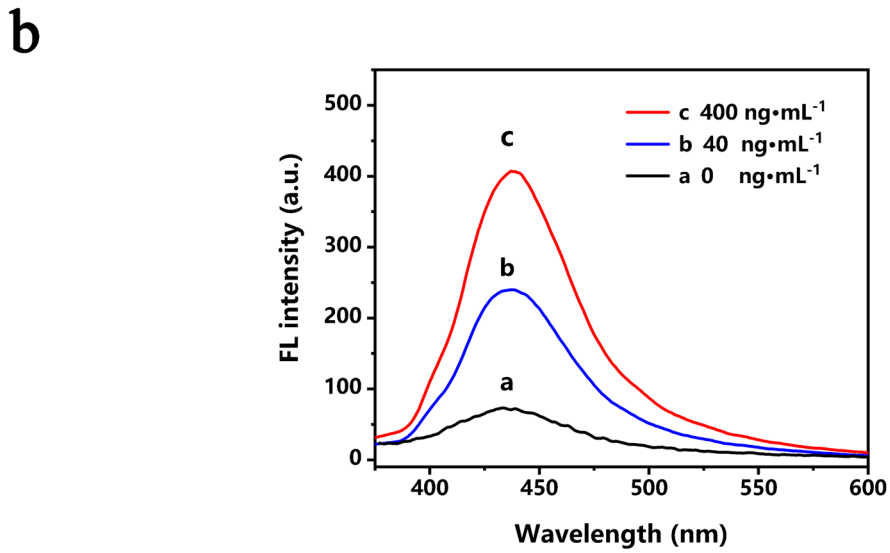

Fig. 4 **a** Schematic illustration of fluorescent aptasensor for GPC3 detection based on aptamer and AuCDs-GPC3$_{Apt}$-Fe_3O_4/GO. **b** The feasibility of fluorescence GPC3 detection based on AuCDs-GPC3$_{Apt}$-Fe_3O_4/GO FRET system (GPC3 concentration: a, 0 ng·mL^{-1}; b, 40 ng·mL^{-1}; c, 400 ng·mL^{-1})

recovery of fluorescence of the AuCDs. The recognition and binding with GPC3 persuaded conformational alteration in aptamer and has reversed the binding of AuCDs-GPC3$_{Apt}$ complex to GPC3-GPC3$_{Apt}$ complex with the discharge of fluorescent AuCDs. In addition, the association constant between the AuCDs-GPC3$_{Apt}$ probes and GPC3 is bigger than that between the AuCDs-GPC3$_{Apt}$ probe probes and Fe_3O_4/GO nanosheets, which leads to AuCDs-GPC3$_{Apt}$ separation from Fe_3O_4/GO nanosheets. The concentration of target GPC3 is quantitatively determined by the changes in fluorescence intensity recorded by spectrophotometer before and after the forming of GPC3-GPC3$_{Apt}$ complex. The fluorescence recovery is positively correlated with GPC3 concentration. This developed aptasensor is rapid and simple since AuCDs and Fe_3O_4/GO were used without functionalization and FRET phenomenon was directly achieved by their intrinsic property.

Then, the feasibility of the GPC3 fluorescence aptasensor was investigated with 40 ng·mL^{-1} and 400 ng·mL^{-1} GPC3 as the experimental group and without GPC3 as the control group, and the results are shown in Fig. 4b. Upon the addition of GPC3 into the AuCDs-GPC3$_{Apt}$-Fe_3O_4/GO FRET system, GPC3 aptamer binds preferentially to GPC3, resulting in conformational changes that impair the synergy of AuCDs-GPC3$_{Apt}$. Due to the magnetic properties of quencher Fe_3O_4/GO, AuCDs-GPC3$_{Apt}$ was magnetically separated from the contact surface. With the increase of the distance between AuCDs-GPC3$_{Apt}$ and Fe_3O_4/GO, the FRET process between them was terminated, and the fluorescence of AuCDs-GPC3$_{Apt}$ was restored. Compared with the control group (0 ng·mL^{-1}, fluorescence intensity: 77), the fluorescence of the experimental group was significantly enhanced with the increase of concentration of GPC3 (40 ng·mL^{-1}, fluorescence intensity: 230; 440 ng·mL^{-1}, fluorescence intensity: 400). The degree of fluorescence recovery is positively correlated with the GPC3 concentration. Therefore, the fluorescence recovery degree can be regarded as the biochemical index of GPC3 concentration to realize high-precision detection.

The feasibility FRET between Fe_3O_4/GO and AuCD$_S$

In order to show the specific properties between the fluorescence donor and the fluorescence acceptor during FRET, Fig. 5a shows the fluorescence emission spectrum of AuCDs-GPC3$_{Apt}$ and the ultraviolet absorption spectrum of Fe_3O_4/GO. The fluorescence emission wavelength of AuCDs-GPC3$_{Apt}$ partially overlaps with the ultraviolet absorption wavelength of Fe_3O_4/GO (400–500 nm), which proves the feasibility of resonance energy transfer between them, and can result in efficient FRET OFF under excitation of a 350 nm laser.

Furthermore, the feasibility of detecting GPC3 by Fe_3O_4/GO and AuCDs was evaluated. The fluorescence intensity of AuCDs-GPC3$_{Apt}$ solution is recorded in three states: initial state, fluorescence quenching state, and fluorescence recovery state (Fig. 5b). The fluorescence intensity of the initial state (AuCDs-GPC3$_{Apt}$) is the highest (Fig. 5b, curve a, peak: 764). After adding Fe_3O_4/GO (2.0 mg·mL^{-1}) to the AuCDs-GPC3$_{Apt}$ solution, the AuCDs-GPC3$_{Apt}$ (fluorescence donor) was adsorbed on the surface of Fe_3O_4/

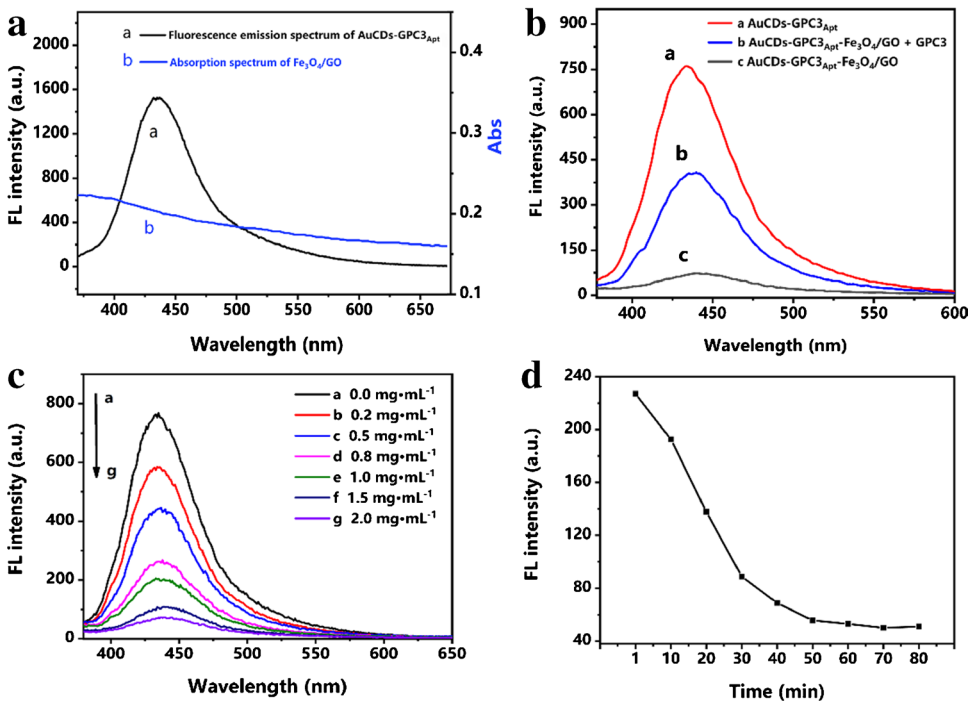

Fig. 5 **a** The ultraviolet-Vis absorption spectrum of Fe_3O_4/GO nanosheets and fluorescence emission spectrum of AuCD$_S$-GPC3$_{Apt}$. **b** Fluorescence emission spectra of AuCDs-GPC3$_{Apt}$ (a, initial state), AuCDs-GPC3$_{Apt}$-Fe_3O_4/GO (c, fluorescence quenching state), and AuCDs-GPC3$_{Apt}$-Fe_3O_4/GO + GPC3 (b, fluorescence recovery state). **c** The quenching effect of Fe_3O_4/GO concentration (0–2.0 mg·mL^{-1}) on the fluorescent aptasensor. **d** Fluorescence emission spectra of AuCDs-GPC3$_{Apt}$-Fe_3O_4/GO in different times

GO (fluorescence receptor) by strong coordination interaction force, and the fluorescence of AuCDs-GPC3$_{Apt}$ was quenched by FRET process. The fluorescence intensity of the fluorescence quenching state (AuCDs-GPC3$_{Apt}$) greatly decreased (Fig. 5b, curve c, peak: 77). However, after adding GPC3 (400 ng·mL^{-1}) to AuCDs-GPC3$_{Apt}$-Fe_3O_4/GO system, the fluorescence was restored to high intensity (Fig. 5b, curve b, peak: 410). In the process, the change in spatial structure caused by the combination of aptamer and GPC3 leads to the magnetic separation of AuCDs-GPC3$_{Apt}$ from Fe_3O_4/GO. The fluorescence of AuCDs-GPC3$_{Apt}$ was recovered because this process blocked FRET. Therefore, we concluded that GPC3 could be sensitively detected based on specific changes of fluorescence intensity.

In order to record the quenching effect of Fe_3O_4/GO on the fluorescent solution, different concentrations of Fe_3O_4/GO were separately added to the same fluorescent solution, and the results are shown in Fig. 5c. With the increase of Fe_3O_4/GO concentration, the fluorescence quenching effect of Fe_3O_4/GO on AuCDs-GPC3$_{Apt}$ is increasing. Therefore, it is feasible to use Fe_3O_4/GO as a quencher in this experiment, and the optimum concentration of Fe_3O_4/GO is 2.0 mg·mL^{-1} (curve g in Fig. 5c).

Figure 5d indicates the time dependence of fluorescence quenching efficiency. The effect of fluorescence quenching is the most obvious in the first 30 min and stabilized after 50 min. In the subsequent fluorescence recovery experiment, 50 min was chosen as incubation time to ensure the best quenching effect.

Optimization of experimental conditions

In order to make the phenomenon of fluorescence recovery more obvious in the experiment, several crucial factors such as incubation time, incubation temperature, pH value of buffer solution, and the concentration of AuCDs-GPC3$_{Apt}$ were optimized. In the experiment, the fluorescence intensity of AuCDs-GPC3$_{Apt}$ after adding Fe_3O_4/GO for fluorescence quenching is denoted as F_0, the fluorescence intensity after adding GPC3 to restore fluorescence in AuCDs-GPC3$_{Apt}$-Fe_3O_4/GO FRET system is denoted as F_1, and the fluorescence recovery rate is expressed as $(F_1 - F_0) / F_0$.

Figure 6a shows the influence of incubation time on the GPC3 fluorescence aptasensor (from 0 to 180 min). Within 140 min, the fluorescence recovery rate of the aptasensor is linearly proportional to incubation time. After 140 min, the fluorescence recovery rate reaches the highest value and remains constant. Therefore, 140 min was selected as the optimum time for incubation GPC3.

Figure 6b shows the influence of incubation temperature on the GPC3 fluorescence aptasensor (from 0 to 50 °C). Within 25 °C, the fluorescence recovery rate increases with the temperature. After 25 °C, the intensity is inversely proportional to the incubation time. Therefore, 25 °C was selected as the optimum incubation temperature for GPC3 detection.

Figure 6c shows the influence of pH on the GPC3 fluorescence aptasensor (from 6.0 to 8.0). Similar to before, the fluorescence recovery rate reaches the peak when the pH value is set to 7.0, the fluorescence recovery effect can be best. So,

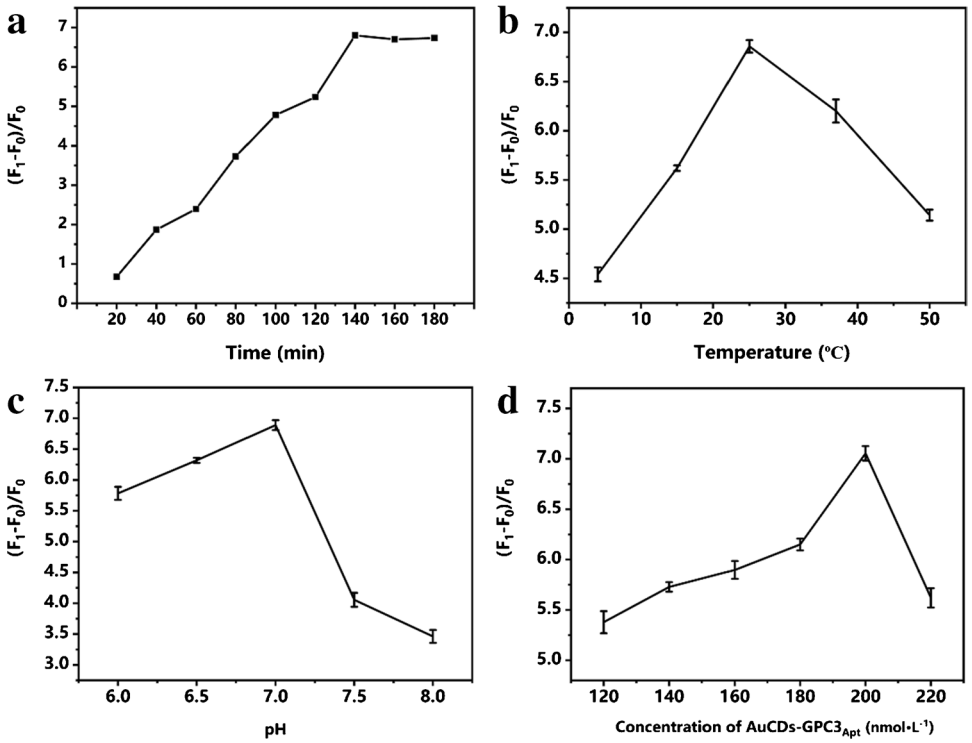

Fig. 6 Optimization of different factors: **a** incubation time, **b** incubation temperature, **c** pH, and **d** concentration of AuCDs-GPC3$_{Apt}$

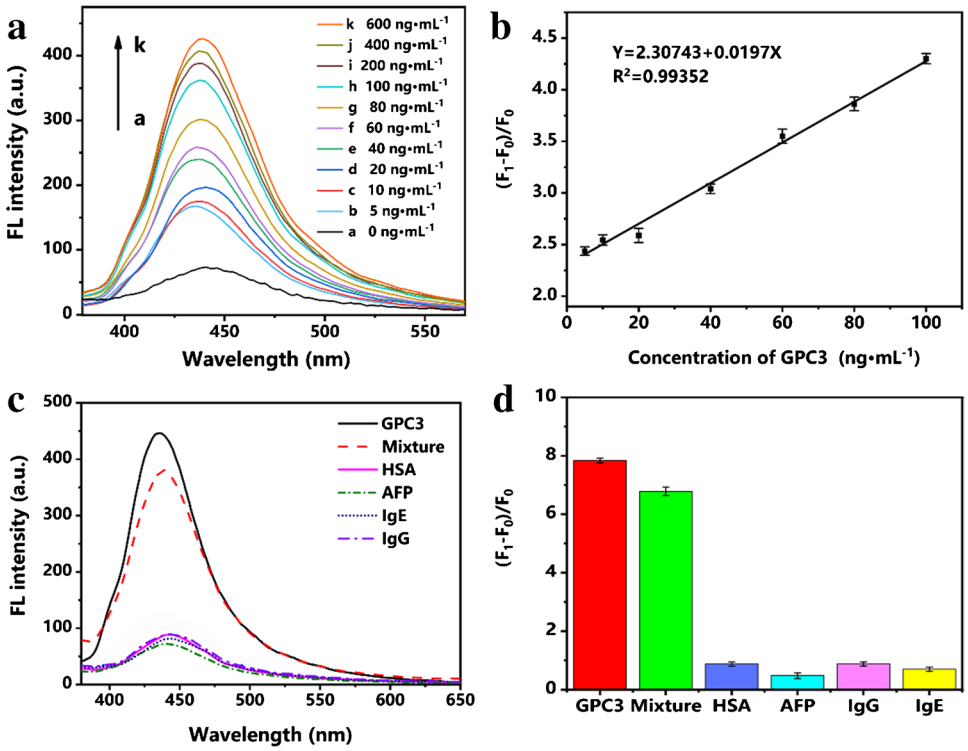

Fig. 7 **a** The fluorescence spectra of the AuCDs-$GPC3_{Apt}$-Fe_3O_4/GO with GPC3 concentrations from 0 to 600 ng·mL^{-1}. **b** The calibration curves between the fluorescence recovery rate and concentrations of GPC3 with the range of 5 to 100.0 ng·mL^{-1}. **c** Fluorescence spectra of different targets (HSA, AFP, IgG, IgE) for the specificity of the proposed GPC3 fluorescence aptasensor. **d** Histogram for the specificity of the proposed GPC3 fluorescence aptasensor. All the above data were presented as average ± SD from three independent measurements and the error bars indicate the relative standard deviation

the optimal pH value is 7.0. There is worth mentioning that the figure (Fig. 6c) is not symmetrical, and the slope on the right is larger indicate that alkaline conditions have a greater influence on fluorescence recovery rate than acidic conditions. Therefore, in order to achieve the best effect of fluorescence recovery rate, it is necessary to make the system non-alkaline.

The fluorescence intensity of the detection system is closely related to the concentration of AuCDs-$GPC3_{Apt}$ (fluorescence donors). Therefore, according to the fluorescence recovery effect, optimization experiments were carried out within the set concentration range of AuCDs-$GPC3_{Apt}$ (120–220.0 nmol·L^{-1}). Figure 6d shows the peak that represents the best fluorescence recovery rate effect appears at 200 nmol·L^{-1}. When the concentration exceeds 200 nmol·L^{-1}, the fluorescence recovery rate shows suddenly drop, which can cause a great interference to the detection process. Therefore, the 200 nmol·L^{-1} of AuCDs-$GPC3_{Apt}$ is selected as the optimum concentration.

As a summary, the following experimental conditions are found to give the best results, the optimal incubation time is 140 min, the optimal incubation temperature is 25 °C, the optimal pH value is 7.0, and the optimal AuCDs-$GPC3_{Apt}$ concentration is 200 nmol·L^{-1}. Thus, the subsequent experiments are carried out under these optimal conditions.

Performance evaluation of the FRET-based fluorescence aptasensor

Under the above optimal conditions, the fluorescence aptasensor was used to detect different concentrations of GPC3 protein (0–600.0 ng·mL^{-1}), and the detection performance was

Table 1 Comparison of the analytical results with a variety of methods for GPC3 detection

Materials	Method	Linear range (ng·mL^{-1})	LOD (ng·mL^{-1})	References
Ig-biotin-GR	DPV	0.75–75	0.2	[10]
AF2119/GPN2-NLuc	BLEIA	1.25–20	1.5	[11]
Affimer-MAb	CLIA	0.03–600	0.03	[12]
GSH/GQDs-$GPC3_{Apt}$	FIA	5–150	2.395	[20]
Anti-GPC3 McAb	TRFIA	1–50	0.039	[48]
Immunoassay kit	ELISA	0.625–40	1.5	[49]
AuCDs-$GPC3_{Apt}$-Fe_3O_4/GO	FIA	5–100	3.01	This work

DPV, differential pulse voltammetry; *BLEIA*, bioluminescence enzyme immunoassay; *CLIA*, chemiluminescence immunoassay; *ELISA*, enzyme-linked immunosorbent assay; *TRFIA*, time-resolved fluorescence immunoassay; *FIA*, fluorescence immunoassay

Table 2 Results of detecting GPC3 in human serum samples using the proposed GPC3 fluorescence apatasensor (measured ($n=3$))

Samples	Added GPC3 concentration ($ng{\cdot}mL^{-1}$)	Measured GPC3 concentration ($ng{\cdot}mL^{-1}$)	RSD%	Recovery%
Normal human serum	10	9.86	2.04%	98.76%
	30	29.78	1.86%	99.28%
	60	60.77	0.53%	101.29%

evaluated by the fluorescence recovery degrees. As shown in Fig. 7a, with the increase of GPC3 protein concentration, the degree of fluorescence recovery gradually increases. Therefore, the quantitative detection of GPC3 protein was realized by calculating the corresponding relationship between fluorescence intensity and GPC3 concentration.

Figure 7b is the calibration plot of the fluorescence aptasensor for different concentrations of GPC3 protein. The fluorescence recovery intensity exhibits a dynamic linear correlation with the concentration of GPC3 protein in the range of 0.0–100.0 $ng{\cdot}mL^{-1}$. The calibration curve is $Y=2.30743+0.0197X$ with the correlation coefficient is 0.99352 (Y is fluorescence recovery rate, X is concentrations of GPC3 protein). The limit of detection (LOD) is calculated to be 3.01 $ng{\cdot}mL^{-1}$ (S/N = 3).

Moreover, Table 1 shows the comparison of determination of GPC3 between the fluorescent method and other techniques in other literatures. Compared with other sensors, our fluorescence aptasensor has a wider linear range, which is more conducive to the practical detection of GPC3. Different from other large-scale detection equipment, the preparation process of aptasensors is simple and convenient, which effectively reduces the cost of constructing a detection system. The Fe_3O_4/GO have the characteristics of abundant oxygen-containing functional groups and high specific surface area, which provide a suitable adsorption site for fluorescence AuCDs quenching. In addition, the aptamer has high affinity and selectivity to the target object, which greatly improves the accuracy and anti-interference of GPC3 detection. The fluorescence detection system based on FRET and aptamers enriches the types of GPC3 detection methods, which can provide a very valuable example for the design of high sensitivity detection methods for clinical application.

Four other interferents (such as HSA, AFP, IgG, and IgE) frequently appear with GPC3 protein were chosen to verify the selectivity of fluorescence aptasensor. The aptasensor was immersed in GPC3 (1.0 $\mu g{\cdot}mL^{-1}$) or the interferents (10.0 $\mu g{\cdot}mL^{-1}$) or the mixture solution (mixture of GPC3, HSA, AFP, IgG, and IgE, the concertration of every substance is 1.0 $\mu g{\cdot}mL^{-1}$) and the fluorescence intensity is detected, and the fluorescence recovery rate is further obtained. As shown in Fig. 7c and Fig. 7d, the interferents showed negligible in fluorescence recovery rate, only the addition of GPC3 protein resulted in a significant recovery in fluorescence intensity, while the addition of other interferents just prompted a slight recovery in fluorescence intensity. For the same concentration, there is few difference in the fluorescence degree recovered between GPC3 and mixture. All in all, the fluorescence aptasensor performed satisfactory selectivity.

Analysis of GPC3 in actual human serum samples

In order to have an intuitive understanding of the measurement of the constructed sensor, the fluorescence aptasensor was used to analysis of GPC3 in human serum. The GPC3 standard solution was spiked into a kind of normal human serum sample. The different spiked samples were measured three times in parallel with the fluorescence aptasensor, and the experimental results are shown in Table 2. The recovery rate of the fluorescence aptasensor is between 98.76 and 101.29%. The RSD value is between 0.53 and 2.04%. These results show that the fluorescence biosensor has a good performance in practicability, which indicates that the sensor had good potential in clinical detection.

Conclusions

In summary, a highly sensitive aptamer-based fluorescent sensing platform for GPC3 detection has been constructed based on the specific binding of $GPC3_{Apt}$ to GPC3 and the FRET between AuCDs and Fe_3O_4/GO. In the presence of GPC3, GPC3 selectively binds to the aptamer of AuCDs-$GPC3_{Apt}$ to form Apt-GPC3, leading to the AuCDs-$GPC3_{Apt}$ detached from the Fe_3O_4/GO nanosheets, thereby interrupting the transfer of FRET and restoring significant recovery of fluorescence of the AuCDs. Under the optimal experimental conditions, the fluorescence recovery rate is linearly correlated with the concentration of GPC3 in the range of 5.0–100.0 $ng{\cdot}mL^{-1}$ with the LOD of 3.01 $ng{\cdot}mL^{-1}$ (S/N = 3). The developed fluorescence aptasensor combines the characteristics of the wide output range, f low cost, high specificity, and strong anti-interference, which would provide a valuable technique for GPC3 detection and good potential in clinical application.

Supplementary Information The online version contains supplementary material available at https://doi.org/10.1007/s00216-022-04201-5.

Funding This work was supported by the National Nature Science Foundation of China (Nos. 62161009 and 82073607), the Open Fund of Guangxi Key Laboratory of Bio-targeting Theranostics (Nos. GXSWBX201902 and GXSWBX201903), and the Open Fund of Guangxi Key Laboratory of Information Materials (No. 211022-K).

Declarations

Ethics approval The human serum samples used in this study were approved by the Guangxi Key Laboratory of Metabolic Diseases Research Ethics Committee in Guilin, China.

Conflict of interest The authors declare no competing interests.

References

1. Huang JJ, Lok V, Ngai CH, Chu C, Patel HK, Chandraseka VT, et al. Disease burden, risk factors, and recent trends of liver cancer: a global country-level analysis. Liver Cancer. 2021;10(4):330–45. https://doi.org/10.1159/000515304.
2. Wang C, Yang L, Liang ZK, Liu YD, Liu SK. Long-term survival and prognostic factors of pulmonary metastasectomy in liver cancer: a systematic review and meta-analysis. World J Surg. 2018;42(7):2153–63. https://doi.org/10.1007/s00268-017-4431-7.
3. Pelizzaro F, Cardin R, Penzo B, Pinto E, Vitale A, Cillo U, et al. Liquid biopsy in hepatocellular carcinoma: where are we now? Cancers (Basel). 2021;13(9):2274. https://doi.org/10.3390/cancers13092274.
4. Galle PR, Foerster F, Kudo M, Chan SL, Llovet JM, Qin SK, et al. Biology and significance of alpha-fetoprotein in hepatocellular carcinoma. Liver Int. 2019;39(12):2214–29. https://doi.org/10.1111/liv.14223.
5. Singal AG, Lampertico P, Nahon P. Epidemiology and surveillance for hepatocellular carcinoma: new trends. J Hepatol. 2020;72(2):250–61. https://doi.org/10.1016/j.jhep.2019.08.025.
6. Li N, Spetz MR, Ho MT. The role of glypicans in cancer progression and therapy. J Histochem Cytochem. 2020;68(12):841–62. https://doi.org/10.1369/0022155420933709.
7. Chen CL, Huang XM, Ying ZJ, Wu DM, Yu YN, Wang XD, et al. Can glypican-3 be a disease-specific biomarker? Clin Transl Med. 2017;6:18. https://doi.org/10.1186/s40169-017-0146-5.
8. Zhou FB, Shang WT, Yu XL, Tian J. Glypican-3: a promising biomarker for hepatocellular carcinoma diagnosis and treatment. Med Res Rev. 2018;38(2):741–67. https://doi.org/10.1002/med.21455.
9. Gao W, Tang ZW, Zhang YF, Feng MQ, Qian M, Dimitrov DS, et al. Immunotoxin targeting glypican-3 regresses liver cancer via dual inhibition of Wnt signalling and protein synthesis. Nat Commun. 2015;6:6536. https://doi.org/10.1038/ncomms7536.
10. Ma X, Wang X, Chen M, Li F. Study on a new high affinity anti-glypicans-3 antibody in diagnosis of early hepatocellular carcinoma by differential pulse voltammetry. J Solid State Electrochem. 2017;21(6):1631–7. https://doi.org/10.1007/s10008-017-3535-1.
11. Yu S, Li ZF, Li JZ, Zhao SM, Wu SG, Liu HJ, et al. Generation of dual functional nanobody-nanoluciferase fusion and its potential in bioluminescence enzyme immunoassay for trace glypican-3 in serum. Sens Actuators B. 2021;336:129717. https://doi.org/10.1016/j.snb.2021.129717.
12. Xie CM, Tiede C, Zhang XY, Wang CR, Li ZX, Xu X, et al. Development of an affimerantibody combined immunological diagnosis kit for glypican-3. Sci Rep. 2017;7:9608. https://doi.org/10.1038/s41598-017-10083-w.
13. Kordasht HK, Hasanzadeh M. Aptamer based recognition of cancer cells: recent progress and challenges in bioanalysis. Talanta. 2020;220:121436. https://doi.org/10.1016/j.talanta.2020.121436.
14. Bayramoglu G, Ozalp VC, Dincbal U, Arica MY. Fast and sensitive detection of salmonella in milk samples using aptamer-functionalized magnetic silica solid phase and MCM-41-aptamer gate system. ACS Biomater Sci Eng. 2018;4(4):1437–44. https://doi.org/10.1021/acsbiomaterials.8b00018.
15. Lu X, Wen X, Fan Z. A sensitive biosensor based on a ferrocene-marked adapter for the fluorescence detection of platelet-derived growth factor BB. J Lumin. 2020;221:117042. https://doi.org/10.1016/j.jlumin.2020.117042.
16. Zhang Y, Lai BS, Juhas M. Recent advances in aptamer discovery and applications. Molecules. 2019;24(5):941. https://doi.org/10.3390/molecules24050941.
17. Bahner N, Reich P, Frense D, Menger M, Schieke K, Beckmann D. An aptamer-based biosensor for detection of doxorubicin by electrochemical impedance spectroscopy. Anal Bioanal Chem. 2018;410(5):1453–62. https://doi.org/10.1007/s00216-017-0786-8.
18. Wu LL, Sedgwick AC, Sun XL, Bull SD, He XP, James TD. Reaction-based fluorescent probes for the detection and imaging of reactive oxygen, nitrogen, and sulfur species. Acc Chem Res. 2019;52(9):2582–97. https://doi.org/10.1021/acs.accounts.9b00302.
19. Guan QH, Li N, Shi LL, Yu CY, Gao XH, Yang JP, et al. Aggregation-induced emission fluorophore-based molecular beacon for differentiating tumor and normal cells by detecting the specific and false-positive signals. ACS Biomater Sci Eng. 2019;5(7):3618–30. https://doi.org/10.1021/acsbiomaterials.9b00627.
20. Li D, Yuan X, Li CN, Luo YH, Jiang ZL. A novel fluorescence aptamer biosensor for trace Pb(II) based on gold-doped carbon dots and DNAzyme synergetic catalytic amplification. J Lumin. 2020;221:117056. https://doi.org/10.1016/j.jlumin.2020.117056.
21. Cao DX, Liu ZQ, Verwilst P, Koo S, Jangjili P, Kim JS, et al. Coumarin-based small-molecule fluorescent chemosensors. Chem Rev. 2019;119(18):10403–519. https://doi.org/10.1021/acs.chemrev.9b00145.
22. Cheng D, Pan Y, Wang L, Zeng ZB, Yuan L, Zhang XB, et al. Selective visualization of the endogenous peroxynitrite in an inflamed mouse model by a mitochondria-targetable two-photon ratiometric fluorescent probe. J Am Chem Soc. 2017;139(1):285–92. https://doi.org/10.1021/jacs.6b10508.
23. Gong PW, Sun L, Wang F, Liu XC, Yan ZQ, Wang MZ, et al. Highly fluorescent N-doped carbon dots with two-photon emission for ultrasensitive detection of tumor marker and visual monitor anticancer drug loading and delivery. Chem Eng J. 2019;356:994–1002. https://doi.org/10.1016/j.cej.2018.09.100.
24. He L, Lu DQ, Liang H, Xie ST, Luo C, Hu MM, et al. Fluorescence resonance energy transfer-based DNA tetrahedron nanotweezer for highly reliable detection of tumor-related mRNA in living cells. ACS Nano. 2017;11(4):4060–6. https://doi.org/10.1021/acsnano.7b00725.
25. Amiri M, Nekoueian K, Saberi RS. Graphene-family materials in electrochemical aptasensors. Anal Bioanal Chem. 2021;413(3):673–99. https://doi.org/10.1007/s00216-020-02915-y.
26. Nanda SS, Papaefthymiou GC, Yi DK. Functionalization of graphene oxide and its biomedical applications. Rev Solid State Mater Sci. 2015;40(5):291–315. https://doi.org/10.1080/10408436.2014.1002604.

27. Zhou Y, Jing X, Chen Y. Material chemistry of graphene oxide-based nanocomposites for theranostic nanomedicine. J Mater Chem B. 2017;5(32):6451–70. https://doi.org/10.1039/c7tb00680b.
28. Mao JN, Hong B, Chen HD, Gao MH, Xu JC, Han YB, et al. Highly improved ethanol gas response of n-type alpha-Fe2O3 bunched nanowires sensor with high-valence donor-doping. J Alloys Compd. 2020;827:154248. https://doi.org/10.1016/j.jallcom.2020.154248.
29. Ge W, Zhang XH, Ge XT, Liu K. Synthesis of alpha-Fe2O3/SiO2 nanocomposites for the enhancement of acetone sensing performance. Mater Res Bull. 2021;141:111379. https://doi.org/10.1016/j.materresbull.2021.111379.
30. Hu LY, Niu CG, Wang XY, Huang DW, Zhang L, Zeng GM. Magnetic separate "turn-on" fluorescent biosensor for bisphenol a based on magnetic oxidation graphene. Talanta. 2017;168:196–202. https://doi.org/10.1016/j.talanta.2017.03.055.
31. Ma L, Guo T, Pan SL, Zhang YH. A fluorometric aptasensor for patulin based on the use of magnetized graphene oxide and DNase I-assisted target recycling amplification. Microchim Acta. 2018;185(10):487. https://doi.org/10.1007/s00604-018-3023-z.
32. Li MK, Hu LY, Niu CG, Huang DW, Zeng GM. A fluorescent DNA based probe for Hg(II) based on thymine-Hg(II)-thymine interaction and enrichment via magnetized graphene oxide. Microchim Acta. 2018;185(3):207. https://doi.org/10.1007/s00604-018-2689-6.
33. Tran CV, La DD, Hoai PNT, Ninh H, Hong PNT, Vu TH, et al. New TiO2-doped Cu-Mg spinel-ferrite-based photocatalyst for degrading highly toxic rhodamine B dye in wastewater. J Hazard Mater. 2021;420:126636. https://doi.org/10.1016/j.jhazmat.2021.126636.
34. Meijer MS, Rojas-Gutierrez PA, Busko D, Howard IA, Frenze F, Wurth C, et al. Absolute upconversion quantum yields of blue-emitting LiYF4: Yb3+, Tm3+upconverting nanoparticles. Phys Chem Chem Phys. 2018;20(35):22556–62. https://doi.org/10.1039/c8cp03935f.
35. Cao CY, Wei P, Li RH, Zhong YP, Li X, Xue FF, et al. Ribosomal RNA-selective light-up fluorescent probe for rapidly imaging the nucleolus in live cells. Acs Sensors. 2019;4(5):1409–16. https://doi.org/10.1021/acssensors.9b00464.
36. Gudimella KK, Appidi T, Wu HF, Battula V, Jogdand A, Rengan AK, et al. Sand bath assisted green synthesis of carbon dots from citrus fruit peels for free radical scavenging and cell imaging. Colloids Surf B. 2021;197:111362. https://doi.org/10.1016/j.colsurfb.2020.111362.
37. Bouche M, Hsu JC, Dong YC, Kim J, Taing K, Cormode DP. Recent advances in molecular imaging with gold nanoparticles. Bioconjug Chem. 2020;31(2):303–14. https://doi.org/10.1021/acs.bioconjchem.9b00669.
38. Mirau PA, Smith JE, Chavez JL, Hagen JA, Kelley-Loughnane N, Naik R. Structured DNA aptamer interactions with gold nanoparticles. Langmuir. 2018;34(5):2139–46. https://doi.org/10.1021/acs.langmuir.7b02449.
39. Nozaki T, Kakuda T, Pottathara YB, Kawasaki H. A nanocomposite of N-doped carbon dots with gold nanoparticles for visible light active photosensitisers. Photochem Photobiol Sci. 2019;18(5):1235–41. https://doi.org/10.1039/c9pp00035f.
40. Zhao ML, Dong LL, Liu Z, Yang SH, Wu WZ, Lin J. In vivo fluorescence imaging of hepatocellular carcinoma using a novel GPC3-specific aptamer probe. Quant Imaging Med Surg. 2018;8(2):151–60. https://doi.org/10.21037/qims.2018.01.09.
41. Li SJ, Wang YN, Mu XQ, Sheng W, Wang JP, Wang S. Two fluorescence quenching immunochromatographic assays based on carbon dots and quantum dots as donor probes for the determination of enrofloxacin. Anal Methods. 2019;11(18):2378–84. https://doi.org/10.1039/c9ay00154a.
42. Figueiredo NM, Carvalho NJM, Cavaleiro A. An XPS study of Au alloyed Al-O sputtered coatings. Appl Surf Sci. 2011;257(13):5793–8. https://doi.org/10.1016/j.apsusc.2011.01.104.
43. Cheng X, Cen Y, Xu GH, Wei FD, Shi ML, Xu XM, et al. Aptamer based fluorometric determination of ATP by exploiting the FRET between carbon dots and graphene oxide. Microchim Acta. 2018;185(2):144. https://doi.org/10.1007/s00604-018-2683-z.
44. Nair RV, Chandran PR, Mohamed AP, Pillai S. Sulphur-doped graphene quantum dot based fluorescent turn-on aptasensor for selective and ultrasensitive detection of omethoate. Anal Chim Acta. 2021;1181:338893. https://doi.org/10.1016/j.aca.2021.338893.
45. Heidari F, Mohajeri N, Zarghami N. Targeted design of green carbon dot-CA-125 aptamer conjugate for the fluorescence imaging of ovarian cancer cell. Cell Biochem Biophys. 2022;80(1):75–88. https://doi.org/10.1007/s12013-021-01034-4.
46. Sadighian S, Bayat N, Najaflou S, Kermanian M, Hamidi M. Preparation of graphene oxide/Fe3O4 nanocomposite as a potential magnetic nanocarrier and MRI contrast agent. ChemistrySelect. 2021;6(12):2862–8. https://doi.org/10.1002/slct.202100195.
47. Tufa LT, Oh S, Tran VT, Kim J, Jeong KJ, Park TJ, et al. Electrochemical immunosensor using nanotriplex of graphene quantum dots, Fe3O4, and Ag nanoparticles for tuberculosis. Electrochim Acta. 2018;290:369–77. https://doi.org/10.1016/j.electacta.2018.09.108.
48. Chen JJ, Xie CM, Wang CR, Wan Y, Dong ZN, Li M, et al. Development of a time-resolved fluorescence immunoassay for the diagnosis of hepatocellular carcinoma based on the detection of glypican-3. J Fluoresc. 2017;27(4):1479–85. https://doi.org/10.1007/s10895-017-2087-1.
49. Tahon AM, El-Ghanam MZ, Zaky S, Emran TM, Bersy AM, El-Raey F, et al. Significance of glypican-3 in early detection of hepatocellular carcinoma in cirrhotic patients. J Gastrointest Cancer. 2019;50(3):434–41. https://doi.org/10.1007/s12029-018-0095-2.